Ganglioside G_{M1}-Mediated Amyloid-beta Fibrillogenesis and Membrane Disruption†

Eva Y. Chi, Shelli L. Frey, and Ka Yee C. Lee*

Department of Chemistry, The Institute for Biophysical Dynamics, and the James Franck Institute, University of Chicago, 929 E. 57th Street, Chicago, Illinois 60637

Received October 19, 2006; Revised Manuscript Received November 29, 2006

ABSTRACT: There is increasing evidence that a class of cell membrane glycolipids, gangliosides, can mediate the fibrillogenesis and toxicity of Alzheimer's disease amyloid-β peptide (Aβ). Using lipid monolayers and vesicles as model membranes, we measured the insertion of Aβ into 1,2-dipalmitoyl-*sn*-glycero-3-phosphocholine (DPPC)−ganglioside G_{M1} monolayers to probe Aβ−G_{M1} interactions, imaged the effects of Aβ insertion on monolayer morphology, and measured the rate of Aβ fibril formation when incubated with 1-palmitoyl-2-oleoyl-*sn*-glycero-3-phosphocholine (POPC)−G_{M1} vesicles. Furthermore, the location of Aβ association in the monolayer was assessed by dual-probe fluorescence experiments. Aβ exhibited direct and favorable interactions with G_{M1} as Aβ insertion monotonically increased with G_{M1} concentration, despite increases in monolayer rigidity at low G_{M1} levels. At low G_{M1} concentrations, Aβ preferentially inserted into the disordered, liquid expanded phase. At higher G_{M1} concentrations, Aβ inserted more uniformly into the monolayer, resulting in no detectable preferences for either the disordered or condensed phase. Aβ insertion led to the disruption of membrane morphology, specifically to the expansion of the disordered phase at low G_{M1} concentrations and significant disruption of the condensed domains at higher G_{M1} concentrations. During incubation with POPC vesicles containing physiological levels of G_{M1}, the association of Aβ with vesicles seeded the formation of Aβ fibrils. In conclusion, favorable interactions between Aβ and G_{M1} in the cell membrane may provide a mechanism for Aβ fibrillogenesis *in vivo*, and Aβ-induced disruption of the cell membrane may provide a pathway by which Aβ exerts toxicity.

Alzheimer's disease (AD[1]) is a neurodegenerative disease in which the normally soluble amyloid-β peptide (Aβ) aggregates to form insoluble intracellular deposits composed of fibrils. The result of Aβ aggregation and deposition is neuronal apoptosis, leading to brain tissue injury and death (*1*). In addition to AD, other prevalent neurodegenerative diseases, such as Parkinson's, Huntington's and prion diseases, as well as a wider group of disorders from liver cirrhosis to degenerative eye diseases share the same general pathology, each arising from the aggregation of an associated protein (*1*−*3*). Although it is accepted that the accumulation of monomeric Aβ into insoluble deposits is the primary event driving the pathogenesis of AD (*1*, *4*), the mechanism and driving forces of Aβ fibril formation *in vivo* and the pathway by which Aβ aggregates result in neurotoxicity are not yet well understood.

Studies of Aβ fibrillogenesis *in vitro* have found that Aβ fibril assembly is a nucleation-dependent polymerization process characterized by an initial lag phase (*5*, *6*). It has been proposed that during nucleation, Aβ monomers first reversibly assemble into micelles at concentrations above a critical micelle concentration (CMC), after which fibrils nucleate within these micelles (*6*). The CMC value of Aβ has been reported to range from 17.5 to approximately 100 μM (*6*−*8*). It is unclear, however, the extent to which these *in vitro* studies reflect the pathway of Aβ fibrillogenesis *in vivo*, where Aβ in the cerebral spinal fluid is only in the subnanomolar concentration range (*9*). The type of homogeneous nucleation-dependent fibrillogenesis observed at high Aβ concentrations clearly cannot be the dominant pathway of Aβ aggregation *in vivo*.

Alternatively, Aβ fibrillogenesis may proceed through a heterogeneously induced, or template-assisted, aggregation pathway. Several lines of evidence suggest that Aβ fibrillogenesis may be a cell membrane-associated process, where the interactions between Aβ and membrane lipids have been found to modulate Aβ fibrillogenesis (*10*−*13*). The Aβ peptide is derived from proteolytic processing of transmembrane amyloid precursor protein (APP) during regular cell metabolism (*14*). The peptide is amphiphilic, with a hydrophilic N-terminal region and a hydrophobic C-terminal region that belongs to the transmembrane domain of APP. The

† This work was supported by the Alzheimer's Association (IIRG-9901175) and the American Health Assistance Foundation (A1999057). The experimental apparatus was made possible by a National Science Foundation Chemistry Research Instrumentation and Facilities Program Junior Faculty Grant (CHE-9816513). E.Y.C. was supported by the National Institutes of Health Ruth L. Kirschstein National Research Service Award Individual Fellowship (AG025649). S.L.F. is grateful for the support of a National Science Foundation graduate research fellowship.

* To whom correspondences should be addressed. Phone: (773) 702-7068. Fax: (773) 702-0805. E-mail: kayeelee@uchicago.edu.

[1] Abbreviations: AD, Alzheimer's disease; Aβ, amyloid-beta peptide; DPPC, 1,2-dipalmitoyl-*sn*-glycero-3-phosphocholine; POPC, 1-palmitoyl-2-oleoyl-*sn*-glycero-3-phosphocholine; FM, fluorescence microscopy; TR-DHPE, Texas Red 1, 2-dihexadecanoyl 3-phosphoethanolamine; PBS, Dulbecco's phosphate buffered saline; FMOC, fluorenylmethoxycarbonyl; RP-HPLC, reverse-phase high performance liquid chromatography; MS/MS, mass spectrometry/mass spectrometry; DMSO, dimethyl sulfoxide; LE, liquid-expanded phase; C, condensed phase; AFM, atomic force microscopy; T_m, main transition temperature; DPPG, 1,2-dipalmitoyl-*sn*-glycero-3-[phospho-*rac*-(1-glycerol)].

10.1021/bi062177x CCC: $37.00
Published on Web 01/26/2007

C-terminus of the Aβ peptide is likely to remain located in the cell membrane after it is cleaved from APP (*15*). The concentration of free and pure Aβ in the extracellular space is, therefore, expected to be exceedingly low; experimentally, it was found to be subnanomolar in the cerebral spinal fluid (*9*). Because of the prominent role the cell membrane plays during the lifetime of the Aβ peptide, it is not surprising that the cell membrane could also mediate Aβ behavior during pathological events such as the misfolding and aggregation of Aβ during the pathogenesis of Alzheimer's disease.

It has been shown that the presence of membrane lipids extracted from human brain cells can accelerate Aβ fibrillogenesis and that the composition of lipid membranes defines Aβ−lipid interactions and fibrillogenesis (*13*, *16*, *17*). One characteristic that has been well documented is the effect of lipid head group charge on Aβ−lipid interaction and fibrillogenesis. Compared to zwitterionic or cationic lipids, anionic lipids have been shown to enhance Aβ's association with and insertion into lipid membranes (*11*, *18*, *19*), inducing the formation of β-sheet structures in Aβ (*10*, *11*, *19*), templating the ordering of Aβ at the lipid interface (*20*), and enhancing the formation of Aβ fibrils (*21*, *22*). We report here a detailed study exploring the effect of ganglioside G_{M1} on Aβ−membrane association and fibrillogenesis.

In addition to modulating Aβ folding and fibrillogenesis, the interaction of Aβ with the cell membrane may serve as a pathway by which Aβ exerts neurotoxicity. Although the exact mechanism of Aβ toxicity is still under debate, alterations in ion permeability have been found in cells exposed to protein aggregates. In particular, changes in the intracellular Ca^{2+} levels have been repeatedly reported (*23*−*25*). Modulation of Ca^{2+} levels has been found to be essential in determining the life and death of a cell, where a rise in Ca^{2+} level may trigger apoptosis (*23*). One proposed mechanism leading to these observed biochemical modifications is cell membrane disruption and depolarization mediated by either ion-channel formation (*26*−*28*) or increases in membrane conductance (*29*−*31*), resulting in the alteration of ion homeostasis and disregulation of neuronal signal transduction, leading to cell death (*1*, *32*). A leading hypothesis of the molecular basis of Aβ toxicity claims that misfolded or aggregated Aβ interacts with the cell membrane and disassembles the lipid bilayer structure (*13*). Direct visualization and detection of membrane disruption accompanying the association and insertion of Aβ into lipid monolayers have been reported (*18*, *20*). The effects of different membrane lipid components on Aβ-induced membrane disruption, however, have not been investigated in detail.

There is increasing evidence that a class of cell membrane glycolipids, gangliosides, can mediate the folding, fibril formation, and toxicity of Aβ (*16*, *33*−*36*). Gangliosides, constituting 5−10% of lipids on the outer leaflet of the cell membrane, regulate various physiological events at the cell surface (*37*). A ganglioside-bound Aβ species has been isolated from AD brain homogenates (*38*). Furthermore, these isolated G_{M1}−Aβ complexes have been shown to seed the assembly of soluble Aβ *in vitro* (*38*). From studying Aβ toxicity in PC12 cells, it was found that the depletion of membrane gangliosides and reduction of cholesterol protected the cells from Aβ-induced GTPase activity (*16*). *In vitro* studies showed that Aβ selectively bound to vesicles containing G_{M1}, compared to zwitterionic or acidic vesicles, and accelerated the rate of fibril formation (*33*). However, vesicles containing G_{M1} have also been found to induce stable α-helical structures in Aβ, diminishing Aβ fibril formation (*39*). To fully elucidate the role gangliosides play in mediating Aβ fibrillogenesis and toxicity, one must understand the nature of the Aβ−ganglioside interaction, the effect of gangliosides on Aβ association with the lipid membrane, and the effect of gangliosides on Aβ-induced membrane disruption.

In this study, we investigated the interaction between Aβ and ganglioside G_{M1} and studied the effect of these interactions on the disruption of membrane morphology and formation of Aβ fibrils. Two model membranes systems, Langmuir lipid monolayers and large unilamellar bilayer lipid vesicles, were used. Interactions between Aβ and G_{M1} were assessed by measuring the insertion of Aβ into 1,2-dipalmitoyl-*sn*-glycero-3-phosphocholine (DPPC) monolayers containing different G_{M1} concentrations at constant surface pressure. Simultaneously, the effect of Aβ association and insertion on monolayer morphology and the location of Aβ insertion within the lipid film were monitored with fluorescence microscopy (FM). To test for the effect of Aβ−membrane interaction on Aβ fibril formation, monomeric Aβ was incubated with POPC vesicles containing different amounts of G_{M1}. Changes in vesicle size distribution, amount of unbound soluble Aβ, and the formation of fibrils with respect to incubation time were monitored using a number of analytical techniques.

MATERIALS AND METHODS

Materials. Lipids DPPC, POPC, and ganglioside G_{M1} were purchased from Avanti Polar Lipids (Alabaster, AL). Headgroup-labeled fluorescent dye Texas Red 1, 2-dihexadecanoyl 3-phosphoethanolamine (TR-DHPE) was purchased from Molecular Probes (Eugene, OR). Dulbecco's phosphate buffered saline (PBS) was purchased from Invitrogen Corp. (Carlsbad, CA). Thioflavin-T was purchased from Sigma-Aldrich (St. Louis, MO). All water used was filtered through a Milli-Q Ultrapure water purification system from Millipore (Bedford, MA).

Aβ40 peptide with an amino acid sequence of DAEFRHDSGYEVHHQKLVFFAEDVGSNKGAIIGLMVGGVV was synthesized using 9-fluorenylmethoxycarbonyl (FMOC) chemistry on an Applied Biosystems 433A Peptide Synthesizer (Foster City, CA). Peptides were purified by reverse-phase high performance liquid chromatography (RP-HPLC) on a preparative Zorbax C18 column at 60 °C. Peptide sequence was confirmed by a mass spectrometry-based protein identification method where purified Aβ was first digested with trypsin and followed by RP-HPLC and mass spectrometry/mass spectrometry (MS/MS) analysis. Peptide mass was confirmed by matrix-assisted laser desorption-ionization (MALDI) mass spectrometry, and peptide purity was determined by analytical RP-HPLC to be 90% or higher. Purified Aβ was lyophilized and stored at −20 °C until use. N-terminus fluorescein-labeled Aβ40 was purchased from AnaSpec (San Jose, CA). To ensure the complete dissociation of Aβ into monomers, the peptide was first dissolved in dimethyl sulfoxide (DMSO) to yield a stock solution of 5 mg/mL (*18*, *40*). Importantly, DMSO did not

exhibit any surface activity. The stock Aβ40 solution was subsequently diluted with an appropriate buffer for insertion or vesicle incubation experiments.

Constant Pressure Insertion Assays. Aβ−lipid interactions were investigated by measuring the degree of peptide insertion into a monolayer of a specific lipid composition at constant surface pressure. Insertion experiments were carried out in a custom-made Langmuir trough. Details of the Langmuir trough setup has been described previously (*18*). Briefly, the setup consisted of a Teflon trough, two Teflon barriers whose motions were precisely controlled by a pair of translational stages (UTM100, Newport, Irvine, CA) for symmetric compression, a stationary Wilhelmy balance (Riegler and Kirstein, Berlin, Germany) located at the center of the trough to measure surface pressure, and a resistively heated cover glass (Delta Technologies, Dallas, TX) to suppress evaporation and prevent condensation on the microscope objective. The trough was temperature controlled, and all experiments were carried out at 30 ± 0.5 °C. All glassware used for trough experiments were treated with a concentrated sulfuric acid solution of Nochromix (GODAX Laboratories Inc., Cabin John, MD) to ensure the complete removal of surface active impurities.

After calibrating the Wilhelmy plate pressure sensor at 30 °C, 80 mL of aqueous subphase was decanted into the trough. Lipids dissolved in either chloroform (Fisher Scientific, HPLC grade) (e.g., DPPC) or chloroform containing 10% methanol (Fisher Scientific, HPLC grade) (e.g., binary mixtures of DPPC and G_{M1}) were spread at the air/water interface. Unless specified otherwise, lipid spreading solutions contained 0.5 mol % of fluorescent dye TR-DHPE. The system was allowed to equilibrate for 15 min to ensure complete evaporation of the organic solvent, after which the lipid monolayer was compressed at a barrier speed of 0.1 mm/s to 25 mN/m. Although this pressure is slightly lower than the bilayer equivalence pressure of approximately 30 mN/m (*41*), we have shown in our earlier work (*18*) that insertion decreases with increasing monolayer surface pressure for a given lipid composition. The pressure of 25 mN/m was chosen for the current study to amplify any weak interactions between G_{M1} and Aβ on the association and insertion of Aβ into lipid monolayers. Once the desired surface pressure was reached, the pressure was kept constant via a feedback loop. An aliquot of 40 μM Aβ in a matching solution was then injected into the subphase of the trough using an L-shaped syringe underneath the barriers to avoid disturbing the lipid film. Final Aβ concentration in the subphase was 250 nM for all insertion experiments. After injecting Aβ, changes in the effective area per lipid molecule ($\Delta A/A = (A_{final} - A_{initial})/A_{initial}$) compared to those before Aβ injection were recorded until the system reached a plateau of no further insertion, which typically took 2−5 h. If no Aβ insertion was observed at 25 mN/m, pressure was reduced at 1 mN/m intervals until insertion occurred.

Visualization of Monolayer Morphology. FM was used to visualize the phase morphology of lipid monolayers and monitor morphological changes of monolayers during Aβ insertion. A Nikon optical microscope (Fryer Co., Huntley, IL) was positioned above the trough and a 50× extra long working distance objective lens was used. A 100 W mercury lamp (Osram Sylvania, Danvers, MA) was used for fluorescence excitation, and a dichroic mirror/filter cube was used to direct light onto the monolayer and to filter the emitted fluorescence. Images were recorded on a digital recorder (Sony GVD 1000 DV Recorder, B & H Photo-Video, New York, NY).

As stated previously, lipid spreading solutions contained 0.5 mol % of head-group-labeled fluorescent lipid dye TR-DHPE. During isothermal compression, the monolayer may undergo a first-order phase transition from a disordered, liquid expanded (LE) phase to an ordered, condensed (C) phase. Because of steric hindrance, the dye partitions into the LE phase of the lipid monolayer, rendering it bright and the C phase dark. Dual probe experiments, where 2.5 mol % of N-terminus fluorescein-labeled Aβ40 (Fl-Aβ) was used in addition to TR-DHPE, were also carried out to pinpoint the location of the inserted and associated Aβ within the lipid film. Fluorescence images were obtained for both fluorophores by switching the filter cube to each of the dye's emission wavelengths. ImageJ (National Institutes of Health) was used to enhance contrast in select images.

Imaging Monolayer with Atomic Force Microscopy. To obtain higher resolution imaging, that is, at the submicron scale, of the effect of Aβ insertion into lipid monolayers, atomic force microscopy (AFM) was used to image monolayers transferred from the air/water interface. Lipid monolayers, with or without inserted Aβ, from the Langmuir trough were transferred onto mica substrates by an inverse Langmuir−Shaefer transfer technique (*42*). A freshly cleaved mica substrate assembly was initially placed in the trough and remained submerged in the subphase during the insertion experiment. After the completion of the experiment, the subphase was aspirated slowly from the trough to lower the subphase level, eventually reaching the mica surface and resulting in the deposition of the monolayer on the substrate. Monolayer morphology before, during, and after transfer was monitored with FM to ensure that the transfer process did not disturb the lipid film. The transferred monolayer was imaged using a Multimode AFM with a J Scanner (Digital instruments, Santa Barbara, CA) in contact mode in air. Silicon nitride tips NP-S (Veeco Probes, Woodbury, NY) were used; the surfaces of the tips were decontaminated by UV generated ozone before sampling (PSD-UV Surface Decontamination System, Novascan, Ames, IA).

Incubation with Large Unilamellar Vesicles. To investigate the effect of Aβ−G_{M1} interaction on Aβ fibril formation, the peptide was incubated with POPC vesicles containing 0, 5, 10, 20, or 30 mol % G_{M1} in water at 25 °C. The monounsaturated lipid POPC was used instead of DPPC because of its lower main transition temperature (T_m), rendering it fluid at 25 °C. DPPC has a T_m of 41 °C (Avanti Polor Lipids) and remains in its gel phase at 25 °C. To prepare lipid vesicles, desired amounts of POPC and G_{M1} were first dissolved in chloroform containing 10% methanol, dried under a stream of nitrogen, and further dried under vacuum overnight. The lipids were then hydrated with water, put through five freeze−thaw cycles, and extruded 19 times using an extruder with 100 nm pore size polycarbonate membranes (Avanti Polar Lipids, Alabaster, AL) to yield large unilamellar vesicles.

Stock Aβ40 dissolved in DMSO was added to each vesicle solution to yield incubation mixtures containing 100 μM Aβ with 1:20 peptide to lipid mole ratio. Samples with a lower Aβ concentration of 25 μM were also prepared with peptide

to lipid ratios ranging from 1:5 to 1:80. Samples were then incubated at 25 °C without agitation. Control samples of Aβ alone and vesicles alone were also prepared and incubated. At each time point, an aliquot of each sample was taken, and the distribution of vesicle size, the amount of soluble peptide remaining, and the presence of fibrils were determined using the analytical methods described below.

Analytical Methods. To evaluate changes in vesicle size during incubation with Aβ, the size distribution of samples and controls were measured by dynamic light scattering using a PD2000DLS detector (Precision Detectors, Franklin, MA). Samples were diluted 500-fold with water, and scattering data were taken for 10 min.

To assess the extent of soluble Aβ depletion from solution due to adsorption onto vesicles or fibril formation, the amount of soluble Aβ remaining in each sample was analyzed by size exclusion HPLC. Samples were first centrifuged at 15,000 rpm for 15 min to remove insoluble materials. A supernatant was then injected onto a BioSep-SEC-S2000 column (Phenomenex, Torrance, CA). Chromatograms were collected as UV absorbance at 215 and 280 nm. The peak area in the chromatogram was used to quantify the amounts of soluble Aβ in the samples. The amount of protein present was calculated by dividing the measured peak area by the peak area for an unincubated control sample.

To monitor the formation of Aβ fibrils, Thioflavin-T fluorescence of incubated samples was measured on a Flouromax-3 spectrofluorometer (Horiva Jobin Yvon, Edison, NJ). Thioflavin-T is known to associate rapidly with aggregated fibrils, giving rise to a new excitation maximum at around 450 nm and enhanced emission at around 482 nm (*43*). At each time point, 20 μL of each sample was mixed with 2 mL of 10 μM Thioflavin-T in PBS, and fluorescence emission intensity was immediately recorded for 10−30 min ($\lambda_{Ex} = 446 \pm 3$ nm, $\lambda_{Em} = 490 \pm 10$ nm) (*40*). Thioflavin-T fluorescence of control samples, Aβ alone and vesicles alone, were also collected to enable proper background subtraction.

To image the structure of the Aβ aggregates formed, transmission electron microscopy (TEM) was used. Samples (5 μL aliquots) were applied to a glow-discharged carbon-coated support film, washed with water, and stained with 1% uranyl acetate for 30 s. Micrographs were recorded using a FEI Tecnai F30 scanning transmission electron microscope (FEI Company, Hillsboro, OR) at magnifications of 15,000×, 49,000×, and 98,000×. The CCD camera provided an additional magnification of all images of 1.4 times.

RESULTS

Effect of G_{M1} on Aβ Insertion into DPPC Monolayers. The interaction between Aβ and lipid monolayers containing G_{M1} was investigated by the monolayer expansion method (*18*, *44*). Lipid monolayers were used to model the outer leaflet of a bilayer membrane. Additionally, the use of monolayers enabled us to test the full range of G_{M1} concentrations, from 0 to 100%, which can amplify any weak protein−lipid interactions that may be present at biologically relevant G_{M1} concentrations or lipid packing density. Figure 1A shows the pressure−area isotherm of DPPC monolayers containing different concentrations of G_{M1} during the compression of lipid monolayers, injection of Aβ, and the insertion of Aβ (arrows in Figure 1A). After compressing a monolayer to

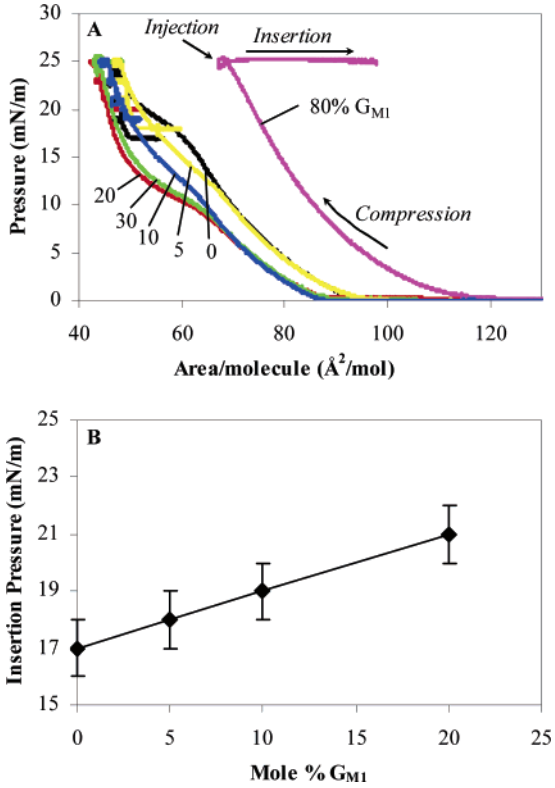

FIGURE 1: (A) Pressure−area isotherms of DPPC monolayers containing different mole % of G_{M1} during the insertion of Aβ at constant pressure. Different stages of the experiment, compression, injection of Aβ, and monolayer expansion due to the insertion of Aβ, are indicated by arrows for the 80% case. For clarity, some isotherms were omitted. (B) Maximum surface pressure at which Aβ insertion occurred at low concentrations of G_{M1}. At these concentrations, no insertion occurred at 25 mN/m. Pressure was lowered by 1 mN/m increments until insertion was observed. All experiments were conducted with an Aβ concentration of 250 nM in water subphase at 30 °C.

25 mN/m, Aβ was injected into the aqueous subphase (final concentration 250 nM) and allowed to equilibrate between the subphase and the lipid monolayer. Favorable interactions between Aβ and lipids led to the adsorption and insertion of Aβ into the lipid monolayer. Under constant pressure conditions, insertion resulted in the expansion of the lipid monolayer (Figure 1A). At low G_{M1} levels, 0−20 mol %, no insertion was observed at 25 mN/m. Monolayer pressure was reduced, by 1 mN/m increments with 15−30 min of equilibration time at each pressure, until insertion was observed. As the G_{M1} concentration in the DPPC monolayer was increased from 0 to 20% (Figure 1B), the maximum pressure at which Aβ inserted into the monolayer increased from 17 to 21 mN/m. Note that the equilibrium spreading pressure, that is, the surface pressure achieved from the equilibrium adsorption of Aβ to a bare air/water interface, was approximately 15 mN/m. For monolayers containing 30 or more mole % of G_{M1}, Aβ insertion occurred at 25 mN/m (Figure 1A).

To fully understand the effect of G_{M1} on Aβ insertion into DPPC monolayers, G_{M1}'s influence on monolayer properties, that is, isotherm and morphology, needs to be elucidated. As shown by the compression isotherms in Figure 1A, G_{M1} induced two changes in the monolayer isotherm: lift-off area and phase-transition pressure. Pure DPPC monolayer showed a characteristic lift-off area of 94 Å^2 per lipid molecule (black

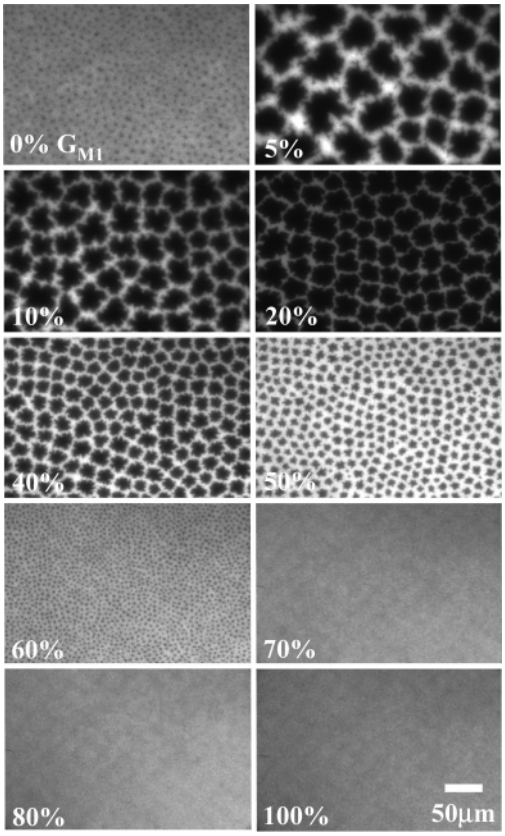

FIGURE 2: Fluorescence micrographs showing the domain morphology of DPPC monolayers containing different mole % of G_{M1} at 25 mN/m and 30 °C. The condensed domains are dark, and the bright regions are the liquid-expanded phase. The scale bar is 50 μM.

line in Figure 1A), where lipids transitioned from a gas/LE coexistence phase to a LE phase. The DPPC isotherm also exhibited a plateau around 19 mN/m, where the monolayer underwent a LE to C phase transition (Figure 1A). The addition of a low concentration of G_{M1} shifted the isotherm to the left (5−20% G_{M1} in Figure 1A), then higher amounts of G_{M1} reversed the trend and shifted the isotherm to the right (>30% G_{M1}, Figure 1A). At higher pressures, these effects of G_{M1} on DPPC isotherms were amplified and, therefore, could be more easily visualized in the area/lipid molecule values. For instance, at 15 mN/m, area per lipid molecule in the absence of G_{M1} was 63.2 Å^2/mol, but decreased to 60.0, 55.0, and 48.9 Å^2/mol for 5, 10, and 20% G_{M1}, respectively, whereas samples with 30, 80, and 100% G_{M1} resulted in increases in area of 50.3, 79.1, and 84.5 Å^2/mol, respectively. This bimodal trend was also observed for the LE to C phase transition, where the increasing G_{M1} concentration first decreased and then increased the phase transition pressure (Figure 1A). At concentrations above 50% G_{M1}, no phase transition plateau was observed during compression to 25 mN/m.

Fluorescence micrographs reflecting the morphology of DPPC monolayers containing different levels of G_{M1} at 25 mN/m are shown in Figure 2. The dark patches represent C domains where bulky head-group-labeled TR-DHPE dye molecules were excluded, and the bright region represents the LE phase where the dye preferentially resided. With increasing G_{M1} concentration, the area fraction of the C domains first increased (5−20% G_{M1}) and then decreased

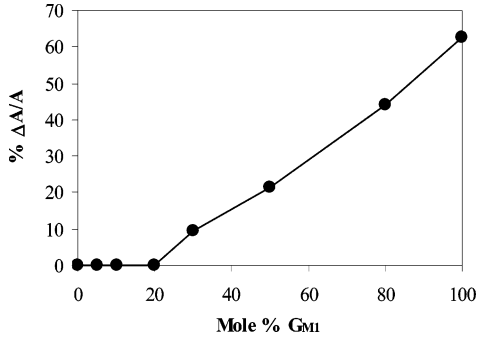

FIGURE 3: Relative area increase (% $\Delta A/A$) of lipid films because of the insertion of Aβ at 25 mN/m and 30 °C as a function of G_{M1} concentration. At low concentrations of G_{M1} (0−20%), Aβ did not insert into DPPC monolayers at 25 mN/m. At higher levels of G_{M1} (>30%), insertion at 25 mN/m increased with increasing G_{M1} levels.

(>30% G_{M1}) (Figure 2). At G_{M1} levels higher than 50%, no condensed domains were observed at a pressure of 25 mN/m. These morphological changes accurately reflected changes observed in compression isotherms (Figure 1A). Taken together, it can be concluded that low concentrations of G_{M1} (5−20%) exerted a condensing effect on the DPPC monolayer, increasing the rigidity of the monolayer, and high concentrations of G_{M1} (>30%) reversed the trend and exerted a fluidizing effect on the lipid monolayer. At G_{M1} concentrations above 50%, the monolayer remained completely fluid, with no apparent LE to C transition, for pressures up to 25 mN/m.

The effect of G_{M1} on the extent of Aβ insertion into DPPC monolayers at 25 mN/m are summarized in Figure 3. As stated previously, no insertion occurred at G_{M1} concentrations less than 20% at this pressure. However, maximum insertion pressure increased with increasing G_{M1} levels in this concentration range (Figure 1B). At G_{M1} concentrations above 30%, Aβ insertion increased with increasing G_{M1} concentration at 25 mN/m (Figure 3). These results suggest that the insertion propensity of Aβ into the DPPC monolayer monotonically increases with increasing G_{M1} concentration.

Effect of pH and Ionic Strength on Aβ Insertion. To better understand the nature of Aβ−G_{M1} interactions, the effect of pH and ionic strength on the insertion of Aβ into a DPPC monolayer containing 50% G_{M1} was tested (Table 1). On a pure water subphase, where the ionic strength was essentially zero and pH was 5.5, Aβ insertion measured at 25 mN/m reached a $\Delta A/A$ of 22%. Note that 25 mN/m was not the maximum insertion pressure. Increasing the ionic strength by the addition of 10 mM buffering salt sodium acetate at pH 5.5 reduced Aβ insertion propensity, where insertion did not occur at 25 mN/m; a maximum insertion pressure of 23 mN/m was measured. Further increasing the ionic strength at pH 5.5 by the addition of 140 mM sodium chloride decreased the insertion pressure to 20 mN/m. Increasing the pH from 5.5 to 6.4 and 7.2, in the presence of 10 mM of buffer salts, decreased the maximum insertion pressure from 23 to 21 and 14 mN/m, respectively. Increasing subphase ionic strength at pH 7.2 by the addition of 140 mM of sodium chloride increased maximum insertion pressure slightly, from 14 to 15 mN/m. Note that the equilibrium spreading pressures of Aβ40 for water and PBS subphase at pH 7.2 were 14.8 and 14.9 mN/m, respectively.

The effect of pH and ionic strength on Aβ insertion can be explained by the electrostatic interactions between Aβ

Table 1: Effect of pH and Ionic Strength on Aβ Insertion into the DPPC Lipid Monolayer Containing 50% G_{M1}

subphase solution condition			maximum Aβ40 insertion pressure (mN/m)	$\Delta A/A$ (%)
pH	salts	ionic strength (M)		
5.5	none	~0	25[c]	22
5.5	10mM NaAc[a]	0.008	23	16
5.5	10mM NaAc 140mM NaCl	0.148	20	11
6.4	10mM NaPh[b]	0.013	21	10
7.2	10mM NaPh	0.024	14	12
7.2	10mM NaPh 140mM NaCl	0.164	15	19

[a] Buffering salt sodium acetate. [b] Buffering salt sodium phosphate. [c] Note that this is not the maximum insertion pressure for this subphase condition. This is the specified pressure at which this insertion experiment was carried out.

and G_{M1}. The head group of G_{M1} contains a sialic acid group (p*K*a = 2.6) that is negatively charged in the 5.5−7.2 pH range. The estimated net charges on Aβ40 on the basis of its amino acid sequence at pH 5.5, 6.4, and 7.2 are 0.2, −1.3, and −2.8, respectively (Protein Calculator v3.3, The Scripps Research Institute). Therefore, attractive electrostatic interactions are expected between Aβ and G_{M1} head groups at pH 5.5. This was experimentally observed, where in a low salt subphase at pH 5.5 (e.g., pure water), attractive electrostatic interactions led to Aβ insertion at 25 mN/m, a pressure that is much higher than the Aβ surface pressure. Increasing ionic strength at pH 5.5 shielded the attractive electrostatic interactions, and decreases in insertion pressure were indeed observed. Increasing pH from 5.5 to 6.4 and 7.2 changed the charge on Aβ from being slightly positive to overall negative. In the same pH range, electrostatic interaction between Aβ and G_{M1} is expected to change from being attractive to repulsive. Experimentally, Aβ insertion pressure decreased sharply with increasing pH. At pH 7.2, insertion pressure of 14 mN/m was slightly lower than the peptide equilibrium surface pressure of 14.9 mN/m, indicative of the repulsive interaction between the peptide and the lipid monolayer that prevented Aβ from adsorbing to the air/subphase interface. Increasing ionic strength with the addition of sodium chloride shielded these repulsive electrostatic interactions between Aβ and G_{M1}, raising the insertion pressure slightly, and reaching that of Aβ equilibrium surface pressure.

Changes to Monolayer Morphology during Aβ Insertion. The morphological changes of monolayers resulting from the insertion of Aβ are shown in Figure 4. Figure 4A shows images captured during the insertion of Aβ into a DPPC monolayer containing 5% G_{M1} at 18 mN/m, the maximum insertion pressure. At the onset of insertion, the monolayer is composed mostly of large condensed domains with finger-like condensed domains protruding from the large domains, forming a network in the disordered LE region (Figure 4A1). This smaller condensed domain network was formed during the expansion of the monolayer that was originally compressed to 25 mN/m. It should be noted that when the film was first compressed to 25 mN/m, the large domains underwent an edge instability at around 22 mN/m as previously described (*45*). The same morphology was observed when a monolayer was first compressed and subsequently expanded on a subphase without Aβ. With the insertion of Aβ at 18 mN/m, the area fraction of the bright disordered region increased (Figures 4A2 and 4A3). In addition, dark condensed domains in the monolayer became disrupted and increasingly irregularly shaped. The insertion of Aβ into the DPPC monolayer containing 20% G_{M1} at 21 mN/m also induced changes in monolayer morphology (Figure 4B). At 8% area expansion due to inserted Aβ, the most prominent change was the disruption of the condensed domain edges (Figure 4B3), rendering them star-shaped. Concomitantly, small condensed domains, dispersed in the disordered domain, appeared. The insertion of Aβ induced similar morphological changes in a DPPC monolayer containing 50% G_{M1} (Figure 4C). With a $\Delta A/A$ of 22%, the edges of condensed domains became disrupted again, producing star-shaped domains (Figure 4C3).

To obtain higher resolution imaging of Aβ induced changes to monolayer morphology, DPPC monolayers with and without inserted Aβ were deposited onto a mica surface by an inverse Langmuir−Shaefer transfer technique (*42*) and imaged in contact mode with AFM. Figure 5A shows the morphology of a pure lipid monolayer (DPPC containing 50% G_{M1}) deposited at 25 mN/m. The monolayer appeared to be made up of hexagonally packed condensed domains with interconnected arms. After an area increase of 22%, monolayer morphology became significantly disrupted (Figure 5B). The round centers of the condensed domains disappeared almost completely, and the interconnected arms that appeared regularly before the insertion of Aβ almost completely vanished. Work is currently underway to better and more completely characterize the rich morphological changes Aβ can induce in phospholipid−G_{M1} monolayers.

Location of Inserted Aβ in Monolayer. To identify the location of inserted Aβ within a lipid monolayer, dual probe fluorescence measurements, using Fl-Aβ in addition to the lipid dye TR-DHPE, were carried out. By switching the filter cubes, fluorescence images of the lipid film were taken at each dye's emission wavelength to correlate the location of peptide with the phase of the lipid monolayer. The fluorescence micrographs in Figure 6 show TR-DHPE fluorescence (images on the left) and Fl-Aβ fluorescence (images in the middle) of the Aβ inserted in a monolayer containing 5% (Figure 6A), 20% (Figure 6B), and 50% (Figure 6C) G_{M1}. For the monolayer containing 5% G_{M1}, with an 18% area change at 18 mN/m, it was clear that the peptide inserted preferentially into the disordered region because the location of FL-Aβ (bright regions in Figure 6A2) coincided with that of TR-DHPE (bright regions of Figure 6A1). For the monolayer containing 20% G_{M1}, with an 8% area change at 25 mN/m, the fluorescence signal from FL-Aβ was much reduced, with little contrast detected within the lipid film (Figure 6B2). Although weak, FL-Aβ fluorescence seemed to correspond to the TR-DHPE signal (Figure 6B1), indicating a weak preference of the inserted Aβ for the disordered phase of the lipid monolayer. This weak contrast in Figure 6B2 can be seen more clearly when the micrograph was adjusted to enhance its contrast (Figure 6B2*). For a monolayer containing a higher percentage of G_{M1}, that is, 50%, no contrast in the fluorescence of FL-Aβ within the lipid monolayer was detected even with enhanment (Figure 6C2*), whereas fluorescence from TR-DHPE clearly showed the existence of small condensed domains in the same film (Figure 6C1). These results indicate that macroscopically,

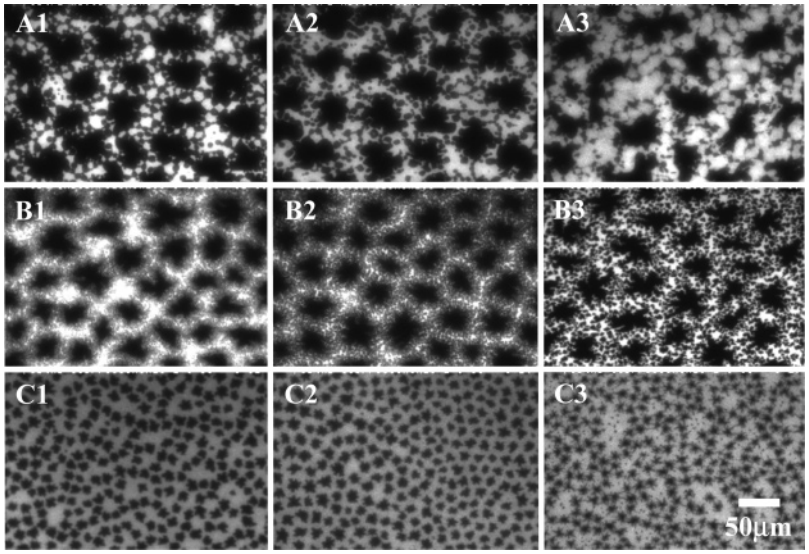

FIGURE 4: Changes in monolayer morphology during the insertion of Aβ into DPPC monolayers containing various amounts of G_{M1}. (A) Morphology of a DPPC monolayer containing 5% G_{M1} at 18 mN/m. From left to right (A1 to A3), the images were captured at 0, 2, and 18% $\Delta A/A$. (B) Morphology of a DPPC monolayer containing 20% G_{M1} at 21 mN/m. From left to right (B1 to B3), the images were captured at 0, 2, and 8% $\Delta A/A$. (C) Morphology of a DPPC monolayer containing 50% G_{M1} at 25 mN/m. From left to right (C1 to C3), the images were captured at 0, 0.2, and 22% $\Delta A/A$. The scale bar is 50 μM.

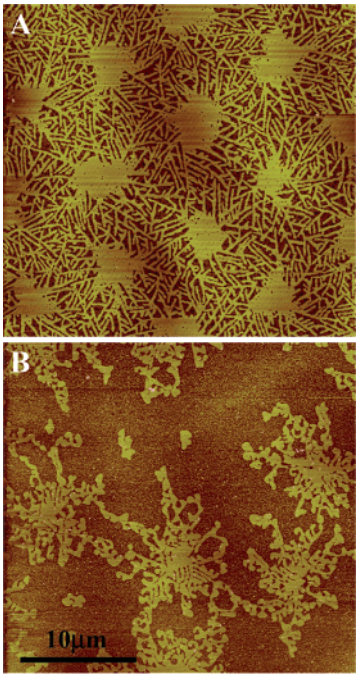

FIGURE 5: AFM images of deposited DPPC monolayers containing 50% G_{M1} before (A) and after (B) Aβ insertion. The monolayers at 25 mN/m were deposited onto a mica surface by an inverse Langmuir−Schaefer transfer technique (*50*).

Aβ within the 50% G_{M1} film was distributed uniformly, with no discernible preference for the disordered or condensed domains.

Effect of G_{M1} on Aβ Fibrillogenesis. To test whether the favorable interactions between Aβ and G_{M1} as measured from a lipid monolayer system would induce the formation of amyloid fibrils, Aβ was incubated with large unilamellar POPC vesicles containing 0, 5, 10, 20, and 30 mol % of G_{M1} at 25 °C.

Figure 7A shows the size distribution of vesicles measured by DLS before (filled circles) and immediately after (open circles) adding Aβ (peptide to protein ratio 1:20). Before the addition of Aβ, the hydrodynamic radius for all vesicles was approximately 70 nm. Immediately after adding Aβ, the size distribution of pure POPC vesicles remained unchanged (Figure 7A). In contrast, the size distribution of POPC vesicles containing 5% G_{M1} became broader and shifted toward larger sizes. Moreover, solutions with vesicles containing higher percentages of G_{M1} became visibly cloudy after the addition of Aβ. Consequently, their size distributions exceeded the detection limit of DLS (Figure 7A). With incubation time, the size distribution of 5% G_{M1} vesicles incubated with Aβ continued to broaden and shift toward larger sizes (Figure 7B).

The amount of soluble Aβ in the incubated samples was measured by SE-HPLC. Samples were first centrifuged to remove any insoluble precipitates, either Aβ bound to vesicles or mature Aβ fibrils. As shown in Figure 8A, the amount of soluble Aβ, which has an elution time of 18 min, decreased with increasing amounts of G_{M1} in the vesicles. The peak detected at 11 min (column void volume) for the pure POPC vesicle sample came from POPC vesicles. No peaks at 11 min were observed for sample containing G_{M1} vesicles because they became associated with Aβ and were removed by centrifugation. Figure 8B shows the percent of soluble Aβ remaining as a function of G_{M1} concentration after 5 or 7 days of incubation. All percentages were relative to 100 μM Aβ at the beginning of incubation. As shown, 100% of soluble Aβ remained when the peptide was incubated alone for 5 or 7 days, indicating that no protein was lost to fibril formation (Figure 8B). The amount of soluble Aβ in samples incubated with pure POPC vesicles also remained at 100% during 7 days of incubation, indicating that no adsorption of Aβ to the vesicle surface or fibril formation occurred (Figure 8B). With increasing G_{M1} concentration in the vesicles, however, the amount of soluble Aβ decreased, indicating the adsorption of protein on the vesicle surface. At G_{M1} concentrations above 20%, essentially all of the Aβ became bound to vesicles. In the samples where only a fraction of the Aβ was adsorbed to the vesicle surface

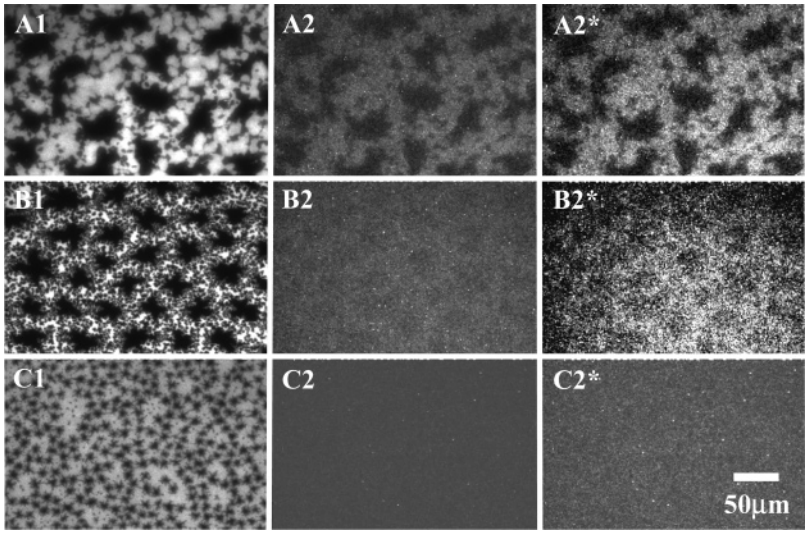

FIGURE 6: Dual probe fluorescence micrographs showing the location of inserted Aβ in the DPPC monolayer containing 5 (A), 20 (B), and 50% (C) G_{M1}. The images on the left (A1, B1, and C1) show fluorescence emission from Texas-Red tagged lipids, and the images in the middle (A2, B2, and C2) show the corresponding fluorescence emission from fluorescein tagged Aβ. Contrast enhanced fluorescein tagged Aβ images are shown on the right (A2*, B2*, and C2*). Experiments were carried out on a water subphase at 30 °C. The images shown were captured with 18% area increase in the 5% G_{M1} monolayer at 18 mN/m (A), 8% area increase in the 20% G_{M1} monolayer at 21 mN/m (B), and 22% area increase in the 50% G_{M1} monolayer at 25 mN/m (C). The scale bar is 50 μM.

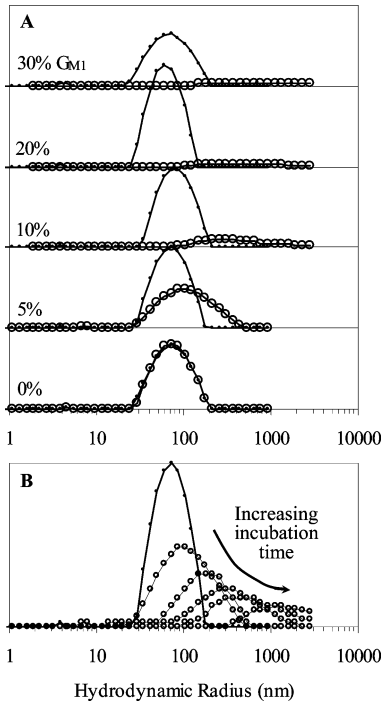

FIGURE 7: Changes in POPC−G_{M1} vesicle size dstribution during incubation with 100 μM Aβ in water at 25 °C. (A) Size distribution of POPC vesicles containing different levels of G_{M1} before (●) and immediately after (○) Aβ was added. (B) Size distribution of vesicles containing 5% G_{M1} (○) as a function of incubation time. Size distribution shifted toward larger sizes with increasing incubation time (0, 1, 2, 4, and 6 days). Vesicles without added Aβ (●) were included for comparison.

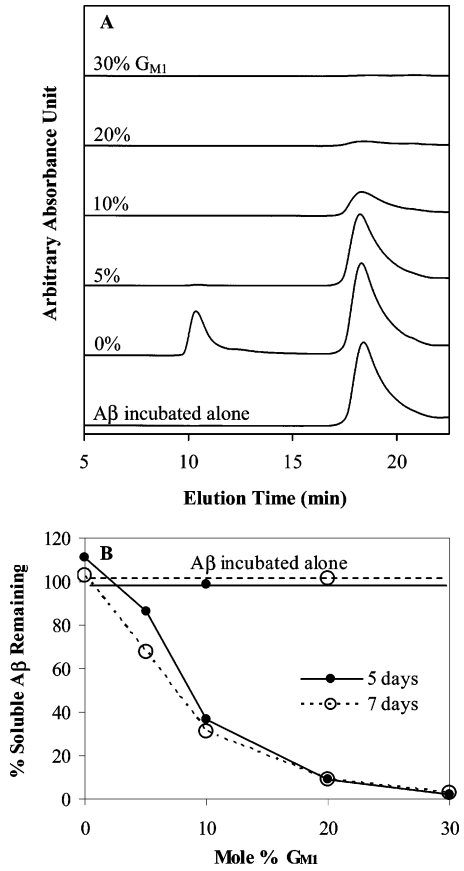

FIGURE 8: (A) Chromatograms of soluble Aβ incubated with vesicles containing different levels of G_{M1} for 5 days. Samples were separated on a size exclusion column, and the absorbance at 215 nm was recorded. Peaks with a retention time of approximately 18 min represent the soluble Aβ fraction. The peak observed at around 11 min coincided with that of the column void volume and was POPC vesicles. (B) Percent of soluble Aβ remaining after 5 (●) and 7 days (○) of incubation with POPC vesicles containing different levels of G_{M1}. For comparison, Aβ incubated alone for 5 (●) and 7 (○) days were also plotted.

(5 and 10% G_{M1}), the soluble protein fraction decreased with incubation time from 5 to 7 days (Figure 8B).

Figure 9 shows Thioflavin-T fluorescence of Aβ incubated with POPC vesicles containing different amounts of G_{M1}. Thioflavin-T is a benzothiazole dye that exhibits enhanced fluorescence upon binding to amyloid fibrils and is commonly used for the detection of amyloid fibrils (*46*, *47*). The

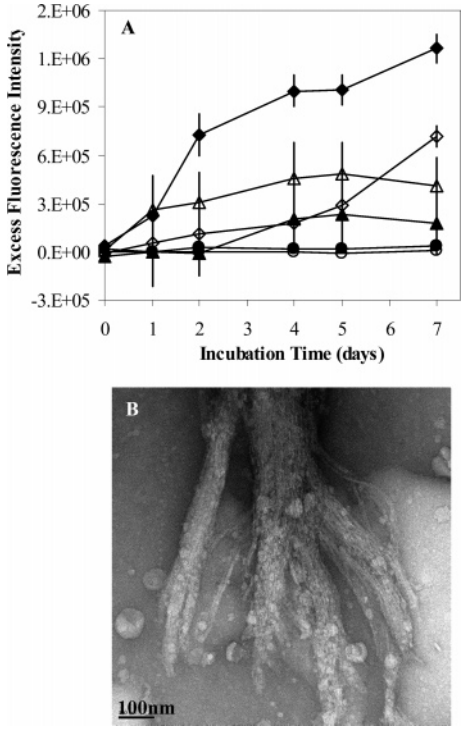

FIGURE 9: (A) Excess Thioflavin-T fluorescence of Aβ incubated with POPC vesicles containing 0 (○), 5 (◇), 10 (♦), 20 (△), and 30% (▲) of G_{M1}. Aβ incubated without any vesicles (●) was also plotted as a control. (B) Transmission electron micrographs of 100 μM Aβ incubated with POPC vesicles containing 5% G_{M1} for 6 days. The scale bar is 100 nm.

control sample, Aβ incubated alone, did not show any increase in fluorescence emission during the 7 days of incubation. The same was observed for Aβ incubated with pure POPC vesicles. However, the rate of fibrillogenesis was greatly increased in the presence of G_{M1}-containing vesicles. When incubated with 5% G_{M1}-containing vesicles, the intensity of Thioflavin-T fluorescence initially increased slowly, then accelerated at longer incubation times (open diamond in Figure 9). Aβ incubated with 10% G_{M1}-containing vesicles showed an initial steep increase in fluorescence followed by slower increases in fluorescence intensity (filled diamonds in Figure 9). When incubated with higher concentrations of G_{M1}-containing vesicles, 20 and 30%, there were initial increases in Thioflavin-T fluorescence, and then the intensity stayed approximately unchanged with longer incubation times.

To confirm that the increase in Thioflavin-T fluorescence of incubated Aβ samples came from fibrillar aggregates, TEM was used to provide high resolution images of the aggregates in incubated samples. Figure 9B shows the transmission electron micrographs of Aβ incubated with POPC vesicles containing 5% G_{M1} for 6 days. The micrograph shows the end of a bundle of laterally assembled, linear, and unbranching fibrils that are approximately 10 nm in diameter. The length of the fibrils reached approximately 3 μm (image not shown).

Aβ was also incubated at a lower concentration of 25 μM with lipid vesicles containing 5 or 10% G_{M1} with peptide to lipid ratios ranging from 1:5 to 1:80. Similar trends in vesicle size distribution, Aβ adsorption, and fibril formation were observed for this lower-Aβ-concentration incubation compared to samples incubated at 100 μM Aβ (data not shown). Aβ did not adsorb to pure POPC vesicles, and the amount of Aβ adsorbed to vesicles increased with increasing amounts of G_{M1} present. The adsorption of Aβ to vesicles led to increases in vesicle size distribution and Thioflavin-T fluorescence.

DISCUSSION

Although our knowledge of protein misfolding, aggregation, and the pathogenesis of neurodegenerative diseases is increasing, the fundamental mechanism of protein fibrillogenesis *in vivo* and the molecular pathway by which protein aggregates exert neurotoxicity have yet to be elucidated. The assembly of monomeric Aβ peptide into fibrillar deposits, which is implicated in the pathogenesis of Alzheimer's disease, is accompanied by substantial changes to the conformation of the peptide, from being primarily α-helical in its native lipidic environment to adopting β-sheet structures in fibrils. *In vivo*, the fibrillogenesis and deposition of Aβ takes place over long periods of time at subnanomolar Aβ concentrations (*9*). *In vitro*, Aβ fibril formation proceeds through a nucleation-dependent aggregation mechanism at concentrations in the range of hundreds of micromolars (*5*, *6*). The underlying cause of the difference in the orders of magnitude of the concentration between *in vivo* and *in vitro* Aβ aggregation may stem from its interactions with its environment.

The lipid membrane has been shown to induce Aβ fibrillogenesis (*10*, *11*, *19*, *21*, *22*), and the disruption of the lipid membrane has been hypothesized as a pathway by which Aβ exerts toxicity (*13*). The effect of different lipids on the type, strength, and mode of interaction between Aβ and the lipid membrane and Aβ fibrillogenesis has not been fully explored. Additionally, only scant data on the characterization of Aβ disruption of the lipid membrane are currently available. In this study, we examined the role a glycolipid ganglioside G_{M1}, whose complex with Aβ has been isolated from AD patients (*38*), plays in modulating the interaction of Aβ with the lipid membrane and its effect on Aβ fibril formation and membrane disruption. Furthermore, by directly visualizing the changes in membrane morphology during Aβ association, we characterized the effect of G_{M1} on membrane disruption induced by Aβ.

G_{M1} Enhanced the Insertion of Aβ into the Lipid Membrane. To probe the interaction between Aβ and G_{M1}-containing lipid membranes, we measured the insertion of Aβ into DPPC monolayers containing 0 to 100 mol % G_{M1} under constant surface pressure conditions. The insertion of Aβ into a pure DPPC monolayer did not occur until the surface pressure of the monolayer was lowered to 17 mN/m, approximately 2 mN/m higher than the equilibrium spreading pressure of Aβ. Thus, Aβ exhibited a weakly attractive interaction with the zwitterionic DPPC lipid. Ganglioside G_{M1} was found to exert a condensing effect on the DPPC monolayer at low levels (0−20%) and a fluidizing effect at higher levels (>30%) (Figures 1A and 2). The insertion of Aβ into a lipid monolayer in general is expected to decrease with increasing monolayer rigidity. This was indeed observed for the insertion of Aβ40 into DPPC and 1,2-dipalmitoyl-*sn*-glycero-3-[phospho-*rac*-(1-glycerol)] (DPPG) monolayers, where insertion decreased with increasing monolayer surface pressure (*18*). In the present study, the

insertion propensity of Aβ into lipid monolayers monotonically increased with increasing G_{M1} levels, even at low G_{M1} concentrations where monolayer rigidity increased with G_{M1} concentration. It can thus be concluded that the favorable Aβ−G_{M1} interactions were sufficiently strong that increases in membrane rigidity did not retard Aβ insertion.

The favorable interactions observed between Aβ and G_{M1} on the water subphase was due to, at least in part, the electrostatic interactions between the negatively charged sialic acid group on the G_{M1} head group and the charged amino acids on Aβ. As expected, this electrostatic interaction was found to be highly pH and ionic strength dependent. Aβ−G_{M1} interactions changed from being attractive to repulsive when pH was increased from 5.5 to 7.2, resulting in sharp decreases in the propensity of Aβ insertion into DPPC−G_{M1} monolayers. Aside from electrostatic interactions, hydrogen bonding between Aβ and sugar groups of the G_{M1} head group can also contribute to the favorable interactions between Aβ and G_{M1}-containing membranes.

G_{M1} Induced the Formation of Aβ Fibrils. To test whether the favorable Aβ−G_{M1}interactions can lead to the formation of Aβ fibrils, Aβ was incubated with POPC vesicles containing different mole % of G_{M1}. When incubated alone, Aβ did not form fibrils during incubation at 25 °C for 7 days at 100 μM because no increases in Thioflavin-T fluorescence were observed (Figure 9), and the amount of soluble Aβ remained at 100% (Figure 8B). Incubation with pure POPC vesicles also did not result in Aβ fibril formation (Figure 9). This is expected because Aβ only weakly interacts with the zwitterionic PC lipid in monolayers at bilayer equivalent pressures (*18*). Incubation of Aβ with POPC vesicles containing G_{M1}, however, exhibited increases in Thioflavin-T fluorescence, indicating the formation of fibrils. Thioflavin-T fluorescence increased with time for Aβ incubated with vesicles containing 5 and 10% G_{M1} but remained relatively unchanged with time after the initial increases for Aβ incubated with vesicles containing 20 or 30% G_{M1} (Figure 9).

Incubation of Aβ with vesicles containing low concentrations of G_{M1} (e.g., 5 or 10%) led to the partial adsorption of Aβ (Figure 8B), leaving unadsorbed, soluble Aβ that could undergo polymerization reactions to form fibrils (Figure 9). In contrast, when incubated with vesicles containing higher percentages of G_{M1} (e.g., 20 or 30%), the increased adsorption sites on the vesicle surfaces led to the depletion of all soluble Aβ (Figure 8B), thereby preventing further polymerization reactions from taking place (Figure 9). Thus, our results show that the differences observed in the amount of fibrils formed during the incubation of Aβ with vesicles containing different percentages of G_{M1} were due to the availability of soluble Aβ to undergo fibril formation rather than the effectiveness of Aβ adsorbed to different vesicles in seeding fibril formation. The same trends were observed when Aβ was incubated at a lower concentration of 25 μM with POPC−G_{M1} vesicles. Aβ adsorbed to vesicles containing G_{M1}, leading to increases in vesicle size distribution and fibrillogenesis. Taken together, it is clear that in the presence of G_{M1}-containing vesicles, Aβ first adsorbed to the membrane surface, and the adsorbed Aβ subsequently acted as seeds for soluble Aβ to assemble into fibrils.

G_{M1} Facilitated Aβ Disruption of Lipid Condensed Domains. To investigate Aβ induced membrane disruption as a molecular mechanism of toxicity, we directly visualized the changes in membrane morphology during the association and insertion of Aβ into lipid monolayers. At low G_{M1} concentrations (e.g., 5% G_{M1} in the DPPC monolayer), Aβ preferentially inserted into the more fluid, LE phase of the monolayer (Figure 6A), increasing the area fraction of the LE phase with insertion (Figure 4A). Previously, Ege et al. showed that the insertion of Aβ40 into single component lipid monolayers composed of both C and LE phases resulted in the appearance of a gray phase, stemming from the disruption of condensed domains at the domain boundaries, and ultimately the disappearance of the C domains (*18*). In this study, although the shapes of the C domains became distorted, the condensed phase remained, and the domain boundaries stayed well-defined (Figure 4A). These observations indicate that the preference for Aβ to insert into the LE phase of a DPPC monolayer containing 5% G_{M1} was sufficiently strong that the condensed phase was not significantly disrupted.

At higher G_{M1} concentrations, the location of inserted Aβ became increasingly more uniform within the lipid film (Figure 6B and C). For example, the insertion of Aβ into a DPPC monolayer containing 50% G_{M1} showed no detectable contrast in the fluorescence signal of FL-Aβ even when the monolayer was clearly composed of both LE and C phases (Figure 2). Fluorescence micrographs showed that Aβ insertion resulted not only in the expansion of the LE phase but also in the disruption of the C domains, which became starfish-like in appearance (Figure 4C). Higher resolution imaging of the monolayers by AFM before and after Aβ insertion showed significant disruptions of both fluid and condensed phases in the lipid monolayer (Figure 5).

From the observations above, it can be concluded that the presence of G_{M1} facilitated the insertion of Aβ into the condensed domains of the model lipid monolayer, resulting in the disruption of these domains. In the plasma membrane of cells, glycosphingolipids such as G_{M1} preferentially partition into a more ordered phase, commonly referred to as lipid rafts (*48*). These rafts serve crucial biological functions, such as signal transduction and sorting and trafficking (*49*). It is thus possible that favorable interactions between Aβ and G_{M1} and the ability of Aβ to disrupt these ordered lipid domains as demonstrated in this study can result in the disruption of lipid raft functions, possibly leading to cell death.

In conclusion, we demonstrated that G_{M1} enhanced the association and insertion of Aβ into model lipid membranes. The favorable Aβ−G_{M1} interactions led to the adsorption of Aβ to G_{M1}-containing lipid vesicles, which subsequently induced the formation of Aβ fibrils. This study also documented, for the first time, the effect of G_{M1} on Aβ membrane disruption. We have demonstrated that G_{M1} can facilitate the disruption of condensed domains in a lipid monolayer. Thus, favorable interactions between Aβ and G_{M1} in the cell membrane may provide a mechanism for Aβ fibrillogenesis *in vivo*, and Aβ induced disruption to cell membrane morphology may provide a pathway by which Aβ exerts toxicity.

ACKNOWLEDGMENT

We gratefully acknowledge Hélène Miller-Auer and Stephen C. Meredith of The University of Chicago for their help with peptide synthesis and Yimei Chen at the Electron Microscopy Facility at The University of Chicago for her help with imaging fibrils. We acknowledge the Biophysical Core Facility at The University of Chicago for the use of their Flouromax-3 spectrofluorometer.

REFERENCES

1. Soto, C. (2003) Unfolding the role of protein misfolding in neurodegenerative diseases, *Nat. Rev. Neurosci. 4*, 49−60.
2. Carrell, R. W. (2005) Cell toxicity and conformational disease, *Trends Cell Biol. 15*, 574−580.
3. Stefani, M. (2004) Protein misfolding and aggregation: new examples in medicine and biology of the dark side of the protein world, *Biochim. Biophys. Acta 1739*, 5−25.
4. Hardy, J., and Selkoe, D. J. (2002) Medicine: The amyloid hypothesis of Alzheimer's disease: Progress and problems on the road to therapeutics, *Science 297*, 353−356.
5. Fezoui, Y., and Teplow, D. B. (2002) Kinetic studies of amyloid beta-protein fibril assembly: Differential effects of alpha-helix stabilization, *J. Biol. Chem. 277*, 36948−36954.
6. Lomakin, A., Chung, D. S., Benedek, G. B., Kirschner, D. A., and Teplow, D. B. (1996) On the nucleation and growth of amyloid beta-protein fibrils: Detection of nuclei and quantitation of rate constants, *Proc. Natl. Acad. Sci. U.S.A. 93*, 1125−1129.
7. Sabate, R., and Estelrich, J. (2005) Evidence of the existence of micelles in the fibrillogenesis of beta-amyloid peptide, *J. Phys. Chem. B 109*, 11027−11032.
8. Soreghan, B., Kosmoski, J., and Glabe, C. (1994) Surfactant properties of Alzheimer's A beta peptides and the mechanism of amyloid aggregation, *J. Biol. Chem. 269*, 28551−28554.
9. Seubert, P., Vigo-Pelfrey, C., Esch, F., Lee, M., Dovey, H., Davis, D., Sinha, S., Schlossmacher, M., Whaley, J., Swindlehurst, C., et al. (1992) Isolation and quantification of soluble Alzheimer's beta-peptide from biological fluids, *Nature 359*, 325−327.
10. McLaurin, J., and Chakrabartty, A. (1997) Characterization of the interactions of Alzheimer beta-amyloid peptides with phospholipid membranes, *Eur. J. Biochem. 245*, 355−363.
11. Terzi, E., Holzemann, G., and Seelig, J. (1997) Interaction of Alzheimer beta-amyloid peptide(1−40) with lipid membranes, *Biochemistry 36*, 14845−14852.
12. Yip, C. M., Darabie, A. A., and McLaurin, J. (2002) Abeta42-peptide assembly on lipid bilayers, *J. Mol. Biol. 318*, 97−107.
13. Yip, C. M., and McLaurin, J. (2001) Amyloid-beta peptide assembly: A critical step in fibrillogenesis and membrane disruption, *Biophys. J. 80*, 1359−1371.
14. Haass, C., Schlossmacher, M. G., Hung, A. Y., Vigo-Pelfrey, C., Mellon, A., Ostaszewski, B. L., Lieberburg, I., Koo, E. H., Schenk, D., Teplow, D. B., et al. (1992) Amyloid beta-peptide is produced by cultured cells during normal metabolism, *Nature 359*, 322−325.
15. Duyckaerts, C., Langui, D., Girardot, N., Hanw, J.-J., and Delantour, B. (2004) Neuropahtology of Alzheimer's Disease, as Seen in Fixed Tissues, in *The Living Brain and Alzheimer's Disease* (Hyman, B., Demonet, J. F., and Christen, Y., Eds.) pp 1−15, Springer, New York.
16. Wang, S. S., Rymer, D. L., and Good, T. A. (2001) Reduction in cholesterol and sialic acid content protects cells from the toxic effects of beta-amyloid peptides, *J. Biol. Chem. 276*, 42027−42034.
17. Yip, C. M., Elton, E. A., Darabie, A. A., Morrison, M. R., and McLaurin, J. (2001) Cholesterol, a modulator of membrane-associated A beta-fibrillogenesis and neurotoxicity, *J. Mol. Biol. 311*, 723−734.
18. Ege, C., and Lee, K. Y. C. (2004) Insertion of Alzheimer's A beta 40 peptide into lipid monolayers, *Biophys. J. 87*, 1732−1740.
19. Terzi, E., Holzemann, G., and Seelig, J. (1994) Alzheimer beta-amyloid peptide 25−35: electrostatic interactions with phospholipid membranes, *Biochemistry 33*, 7434−41.
20. Ege, C., Majewski, J., Wu, G., Kjaer, K., and Lee, K. Y. C. (2005) Templating effect of lipid membranes on Alzheimer's amyloid beta peptide, *ChemPhysChem 6*, 226−229.
21. Chauhan, A., Ray, I., and Chauhan, V. P. (2000) Interaction of amyloid beta-protein with anionic phospholipids: possible involvement of Lys28 and C-terminus aliphatic amino acids, *Neurochem. Res. 25*, 423−429.
22. Zhao, H., Tuominen, E. K., and Kinnunen, P. K. (2004) Formation of amyloid fibers triggered by phosphatidylserine-containing membranes, *Biochemistry 43*, 10302−10307.
23. Cecchi, C., Baglioni, S., Fiorillo, C., Pensalfini, A., Liguri, G., Nosi, D., Rigacci, S., Bucciantini, M., and Stefani, M. (2005) Insights into the molecular basis of the differing susceptibility of varying cell types to the toxicity of amyloid aggregates, *J. Cell Sci. 118*, 3459−3470.
24. Dobson, C. M. (2003) Protein folding and misfolding, *Nature 426*, 884−890.
25. Stefani, M., and Dobson, C. M. (2003) Protein aggregation and aggregate toxicity: new insights into protein folding, misfolding diseases and biological evolution, *J. Mol. Med. 81*, 678−699.
26. Arispe, N., Pollard, H. B., and Rojas, E. (1993) Giant multilevel cation channels formed by Alzheimer-disease amyloid beta-protein [a-beta-P-(1−40)] in bilayer-membranes, *Proc. Natl. Acad. Sci. U.S.A. 90*, 10573−10577.
27. Arispe, N., Rojas, E., and Pollard, H. B. (1993) Alzheimer-disease amyloid beta-protein forms calcium channels in bilayer-membranes: blockade by tromethamine and aluminum, *Proc. Natl. Acad. Sci. U.S.A. 90*, 567−571.
28. Quist, A., Doudevski, I., Lin, H., Azimova, R., Ng, D., Frangione, B., Kagan, B., Ghiso, J., and Lal, R. (2005) Amyloid ion channels: a common structural link for protein-misfolding disease, *Proc. Natl. Acad. Sci. U.S.A. 102*, 10427−10432.
29. Demuro, A., Mina, E., Kayed, R., Milton, S. C., Parker, I., and Glabe, C. G. (2005) Calcium dysregulation and membrane disruption as a ubiquitous neurotoxic mechanism of soluble amyloid oligomers, *J. Biol. Chem. 280*, 17294−17300.
30. Deshpande, A., Mina, E., Glabe, C., and Busciglio, J. (2006) Different conformations of amyloid beta induce neurotoxicity by distinct mechanisms in human cortical neurons, *J. Neurosci. 26*, 6011−6018.
31. Kayed, R., Sokolov, Y., Edmonds, B., McIntire, T. M., Milton, S. C., Hall, J. E., and Glabe, C. G. (2004) Permeabilization of lipid bilayers is a common conformation-dependent activity of soluble amyloid oligomers in protein misfolding diseases, *J. Biol. Chem. 279*, 46363−46366.
32. Lashuel, H. A., Hartley, D., Petre, B. M., Walz, T., and Lansbury, P. T., Jr. (2002) Amyloid pores from pathogenic mutations, *Nature 418*, 291.
33. ChooSmith, L. P., GarzonRodriguez, W., Glabe, C. G., and Surewicz, W. K. (1997) Acceleration of amyloid fibril formation by specific binding of A beta-(1−40) peptide to ganglioside-containing membrane vesicles, *J. Biol. Chem. 272*, 22987−22990.
34. Choo-Smith, L. P., and Surewicz, W. K. (1997) The interaction between Alzheimer amyloid beta(1−40) peptide and ganglioside GM1-containing membranes, *FEBS Lett. 402*, 95−98.
35. Hayashi, H., Kimura, N., Yamaguchi, H., Hasegawa, K., Yokoseki, T., Shibata, M., Yamamoto, N., Michikawa, M., Yoshikawa, Y., Terao, K., Matsuzaki, K., Lemere, C. A., Selkoe, D. J., Naiki, H., and Yanagisawa, K. (2004) A seed for Alzheimer amyloid in the brain, *J. Neurosci. 24*, 4894−4902.
36. Kakio, A., Nishimoto, S., Yanagisawa, K., Kozutsumi, Y., and Matsuzaki, K. (2002) Interactions of amyloid beta-protein with various gangliosides in raft-like membranes: importance of GM1 ganglioside-bound form as an endogenous seed for Alzheimer amyloid, *Biochemistry 41*, 7385−7390.
37. Alberts, B., Johnson, A., Lewis, J., Raff, M., Roberts, K., and Walter, P. (2002) *Molecular Biology of the Cell*, 4th ed., Garland Science, Taylor & Francis Group, New York, NY.
38. Yanagisawa, K., Odaka, A., Suzuki, N., and Ihara, Y. (1995) Gm1 ganglioside-bound amyloid beta-protein (Ab): a possible form of preamyloid in Alzheimers-disease, *Nat. Med. 1*, 1062−1066.
39. McLaurin, J., Franklin, T., Fraser, P. E., and Chakrabartty, A. (1998) Structural transitions associated with the interaction of Alzheimer beta-amyloid peptides with gangliosides, *J. Biol. Chem. 273*, 4506−4515.
40. Sciarretta, K. L., Gordon, D. J., Petkova, A. T., Tycko, R., and Meredith, S. C. (2005) Ab40-Lactam(D23/J28) models a conformation highly favorable for nucleation of amyloid, *Biochemistry 44*, 6003−6014.
41. Seelig, A. (1987) Local anesthetics and pressure: a comparison of dibucaine binding to lipid monolayers and bilayers, *Biochim. Biophys. Acta 899*, 196−204.

42. Lee, K. Y. C., Lipp, M. M., Takamoto, D. Y., Ter-Ovanesyan, E., Zasadzinski, J. A., and Waring, A. J. (1998) Apparatus for the continuous monitoring of surface morphology via fluorescence microscopy during monolayer transfer to substrates, *Langmuir 14*, 2567−2572.
43. LeVine, H. (1999) Quantification of Beta-Sheet Amyloid Fibril Structures with Thioflavin T, in *Amyloid, Prions, and Other Protein Aggregates* (Wetzel, R., Ed.) pp 274−284, Academic Press, San Diego, CA.
44. Hanakam, F., Gerisch, G., Lotz, S., Alt, T., and Seelig, A. (1996) Binding of hisactophilin I and II to lipid membranes is controlled by a pH-dependent myristoyl-histidine switch, *Biochemistry 35*, 11036−11044.
45. Diamant, H., Witten, T. A., Ege, C., Gopal, A., and Lee, K. Y. (2001) Topography and instability of monolayers near domain boundaries, *Phys. Rev. E: Stat. Phys., Plasmas, Fluids, Relat. Interdiscip. Top. 63*, 061602−061612.
46. Khurana, R., Coleman, C., Ionescu-Zanetti, C., Carter, S. A., Krishna, V., Grover, R. K., Roy, R., and Singh, S. (2005) Mechanism of thioflavin T binding to amyloid fibrils, *J. Struct. Biol. 151*, 229−238.
47. Krebs, M. R., Bromley, E. H., and Donald, A. M. (2005) The binding of thioflavin-T to amyloid fibrils: localisation and implications, *J. Struct. Biol. 149*, 30−37.
48. Fantini, J., Garmy, N., Mahfoud, R., and Yahi, N. (2002) Lipid rafts: structure, function and role in HIV, Alzheimer's and prion diseases, *Exp. Rev. Mol. Med. 20 December*, http://www.expertreviews.org/02005392h.htm.
49. Brown, D. A., and London, E. (1998) Functions of lipid rafts in biological membranes, *Annu. Rev. Cell Dev. Biol. 14*, 111−136.
50. Lipp, M. M., Lee, K. Y., Waring, A., and Zasadzinski, J. A. (1997) Fluorescence, polarized fluorescence, and Brewster angle microscopy of palmitic acid and lung surfactant protein B monolayers, *Biophys. J. 72*, 2783−2804.

BI062177X